A Timing Mismatch Background Calibration Algorithm With Improved Accuracy

Zhifei Lu, He Tang, Zhaofeng Ren, Ruogu Hua, Haoyu Zhuang, and Xizhu Peng

***Abstract*— This brief presents a novel timing mismatch background calibration algorithm for time-interleaved (TI) analog-to-digital converters (ADCs). It can calibrate an arbitrary number of channels with an arbitrary input frequency. It also increases the calibration accuracy by applying the autocorrelation functions with an expanded interval. Besides, the proposed algorithm effectively prevents the small derivative values in the correlation difference from degrading the skew estimation accuracy. Compared to prior works on calibration, this work has at least five times better detection accuracy when the frequency of the input signal is close to the Nyquist frequency. This is without the need for calculating the high-order statistics. Finally, we simulate a four-channel 12-bit TI ADC with non-ideal effects added. Simulation results show that the proposed algorithm increases the signal to noise-plus-distortion ratio (SNDR) and spurious-free dynamic range (SFDR) from 35.5 and 40.0 dB to 63.3 and 84.6 dB, respectively, when the input frequency is close to the Nyquist frequency.**

***Index Terms*— Arbitrary input frequency, background calibration, blind estimation, time-interleaved (TI) analog-to-digital converter (ADC), timing mismatch.**

I. Introduction

Time interleaving is effective for increasing the speed of analog-to-digital converters (ADCs) [1]. By combining N channels in parallel, the time-interleaved (TI) ADC can achieve an N times faster sampling rate. Nevertheless, the time interleaving suffers from inter-channel mismatches, including the offset mismatch, the gain mismatch, the bandwidth mismatch, and the timing mismatch. These mismatches can lead to nonlinearity and thus degrade the performance of the TI ADC [2]. From this perspective, a mismatch calibration algorithm is indispensable.

Usually, the mismatches are calibrated in the following order [3]: the offset mismatch is calibrated first, and then the gain mismatch, the bandwidth mismatch, and finally the timing mismatch. In [4] and [5], to calibrate the timing mismatch in the background, an extra ADC channel is added as the reference for skew trimming. However, the reference ADC channel requires extra analog design with high complexity, which is undesirable. To calibrate the timing mismatch without reference channel, many techniques apply statistical method to measure the mismatches [3], [6]–[14]. Among them, Huang *et al.* [6] use zero-crossing (ZC) method to detect timing mismatches and use digitally-controlled variable delay lines (VDLs) for compensation. Also, Yin and Ye [7] apply first-order statistics method with digital filters to achieve fast convergence in timing mismatch calibration. Furthermore, autocorrelation functions are widely used [8]–[14]. In [8]–[11], a two-channel-based calibration is applied but it has a drawback that the number of channels is strictly limited to the power of 2. By contrast, Salib *et al.* [12] and Le Duc *et al.* [13] can calibrate an arbitrary number of channels. Nevertheless, it has a drawback that the noise of each channel is accumulated in the timing mismatch estimation, limiting the calibration accuracy. Another drawback is that, in [8]–[14], the calibration accuracy is degraded at some specific input frequencies due to the algorithm itself. This issue is undesirable, because ideally we should be able to perform the calibration at any input frequency with high calibration accuracy.

To address the above issues, this brief proposes a novel timing mismatch calibration algorithm. It calibrates an arbitrary number of channels at an arbitrary input frequency in the background. The algorithm improves the detection accuracy by applying autocorrelation functions with an expanded interval for reducing the impact of noise and high-order terms in Taylor approximation. Also, it effectively prevents the small derivative values in correlation difference from degrading the skew estimation accuracy. Compared to prior works on calibration, the proposed algorithm has at least five times higher accuracy when the input frequency is close to the Nyquist frequency, even without the need for calculating the high-order statistics. Simulation results show that our algorithm increases the signal to noise-plus-distortion ratio (SNDR) and spurious-free dynamic range (SFDR) by 27.8 and 44.6 dB, respectively, even when the input frequency is close to the Nyquist frequency.

This brief is organized as follows. Section II discusses the prior calibration algorithm as well as its drawbacks, and presents the proposed background timing mismatch calibration. Section III shows the simulation results of a four-channel 12-bit TI ADC, which validates the effectiveness of the proposed algorithm. Finally, a conclusion is drawn in Section IV.

II. Proposed Timing Mismatch Calibration Algorithm

A. Mathematical Model of an N-Channel TI ADC With Timing Mismatches

In an N-Channel TI ADC, for simplicity, T_s represents the sampling period of the entire ADC, k represents the channel number ($k = 1, \ldots, N$), and m represents the conversion number of one channel ($m = 0, 1, \ldots, +\infty$). From this perspective, the sampling time can be calculated as $t_{m,k} = (N \cdot m + k) \cdot T_s$. Consider an input signal $x(t_{m,k})$ sampled at $t_{m,k}$, then the ADC output signal $y[n]$ can be expressed as

$$y[n] = y(t_{m,k}) = y((N \cdot m + k) \cdot T_s) \tag{1}$$

where n (=0, 1, …, $+\infty$) is the number of sampling of the entire ADC. If there is a timing mismatch Δt_k in the kth channel, then $t_{m,k} = (N \cdot m + k) \cdot T_s + \Delta t$, and the ADC output signal $y[n]$ becomes

$$y[n] = y((N \cdot m + k) \cdot T_s + \Delta t_k). \tag{2}$$

Manuscript received November 25, 2020; revised March 1, 2021 and April 22, 2021; accepted May 13, 2021. This work was supported in part by the National Natural Science Foundation of China under Grant 62004023 and Grant 61801087, in part by the National Key Research and Development Program of China under Grant 2018YFB2100100, and in part by the Department of Science and Technology of Sichuan Province under Grant 2018GZDZX0002 and Grant 2018GZDZX0003. *(Corresponding author: Xizhu Peng.)*

The authors are with the School of Electronic Science and Engineering, University of Electronic Science and Technology of China, Chengdu 610054, China, and also with the State Key Laboratory of Electronic Thin Films and Integrated Devices, University of Electronic Science and Technology of China, Chengdu 610054, China (e-mail: xzpeng@uestc.edu.cn).

Color versions of one or more figures in this article are available at https://doi.org/10.1109/TVLSI.2021.3082719.

Digital Object Identifier 10.1109/TVLSI.2021.3082719

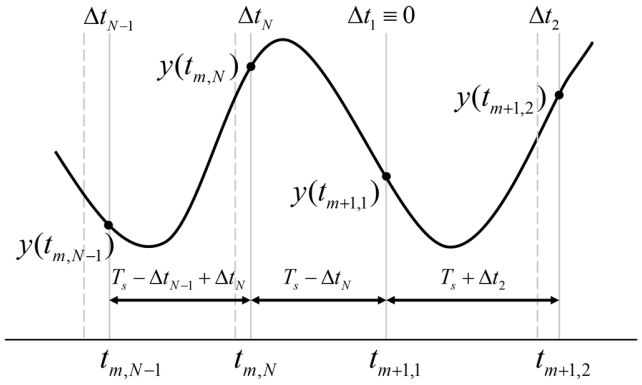

Fig. 1. Influence of timing mismatches in an N-channel TI ADC.

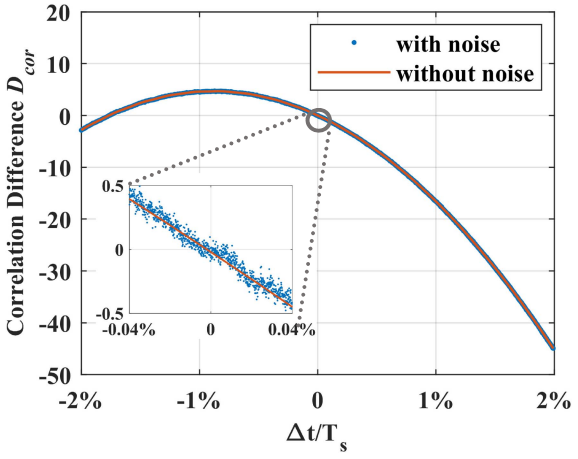

Fig. 2. Correlation difference D_{cor} varies with timing mismatch Δt with noise (blue dot) and without noise (red line).

Besides, more non-ideal effects are added into (2), including the quantization error e_{q}, the thermal noise e_{th}, and the clock jitter e_{j}. Then, the ADC output signal $y[n]$ becomes

$$y[n] = y((N \cdot m + k) \cdot T_s + \Delta t_k + e_j) + e_q + e_{th}. \tag{3}$$

B. Prior Works on Correlation-Based Calibration

The prior work of [8]–[14] multiplies the output of two interleaved channels and uses time average of the product to measure timing mismatches. Because the difference of the time average is proportional to the mismatch Δt [8], the timing mismatches can be easily estimated. The autocorrelation function $R(\tau)$ is used to calculate the product's average, expressed as follows:

$$R(\tau) = E(y[n] \cdot y[n+1]) = E(y(t_{m,k}) \cdot y(t_{m,k} + \tau)). \tag{4}$$

Here, τ is the interval between two samples in the calculation of $R(\tau)$. The ideal value of the interval $\tau = T_{\mathrm{s}}$ is used in the prior work of [12]–[14]. As shown in Fig. 1, the practical interval τ between the $(k-1)$th channel and the kth channel is affected by timing skews Δt_{k-1} and Δt_k, expressed as $\tau = T_{\mathrm{s}} + \Delta t_k - \Delta t_{k-1}$, and $R(\tau) = R(T_{\mathrm{s}} + \Delta t_k - \Delta t_{k-1})$. For simplicity, $R_{k-1,k}$ represents $R(T_{\mathrm{s}} + \Delta t_k - \Delta t_{k-1})$. And this $R_{k-1,k}$ can be approximated as follows, by using the Taylor series:

$$R_{k-1,k} = R(T_{\mathrm{s}}) + R'(T_{\mathrm{s}}) \cdot \Delta t_k - R'(T_{\mathrm{s}}) \cdot \Delta t_{k-1} \tag{5}$$

where $R'(T_{\mathrm{s}})$ denotes the slope or derivative of $R(\tau)$ at $\tau = T_{\mathrm{s}}$. For an N-Channel TI ADC, we choose the first channel as the reference channel as an example. This leads to $\Delta t_1 = 0$.

Therefore, the difference of the time average, which is defined as the correlation difference D_{cor}, can be estimated from the expression in (6). As mentioned before, the $D_{\mathrm{cor-k}}$ is proportional to the timing mismatch Δt_k. Thus, the timing skews can be estimated easily using (6). Then, by using the estimated timing mismatches, the sampling error of the ADC can be calculated as the product of the timing mismatch and the slope of signal [13], [14]

$$\begin{cases} N \cdot R'(T_{\mathrm{s}}) \cdot \Delta t_2 = (N-1) \cdot R_{1,2} - R_{2,3} - \cdots - R_{N,1} = D_{\mathrm{cor-2}} \\ \cdots \\ N \cdot R'(T_{\mathrm{s}}) \cdot \Delta t_k = (N-k+1) \cdot (R_{1,2} + \cdots + R_{k-1,k}) \\ \quad -(k-1) \cdot (R_{k,k+1} + \cdots + R_{N,1}) = D_{\mathrm{cor-k}} \\ \cdots \\ N \cdot R'(T_{\mathrm{s}}) \cdot \Delta t_N = R_{1,2} + R_{2,3} + \cdots - (N-1) \cdot R_{N,1} = D_{\mathrm{cor-N}}. \end{cases} \tag{6}$$

However, the prior works have the limitation that it cannot work well when the input signal frequency f_{in} is close to the zero frequency, the Nyquist frequency $f_{\mathrm{s}}/2$, and its multiples $n_f \cdot f_{\mathrm{s}}/2$ $(n_f = 0, 1, 2, \ldots)$. To explain the reason, a sinusoidal input $x(t) = A \cdot \sin(\omega \cdot t + \varphi)$ is applied as an example, whose autocorrelation function $R(\tau)$ is as follows:

$$R(\tau) = \frac{A^2}{2} \cdot \cos(\omega \cdot \tau) \tag{7}$$

where $\omega = 2\pi f_{\mathrm{in}}$, $T_{\mathrm{s}} = 1/f_{\mathrm{s}}$. The derivative of $R'(T_{\mathrm{s}})$ is as follows:

$$R'(T_{\mathrm{s}}) = -A^2 \cdot f_{\mathrm{in}} \cdot \pi \cdot \sin\left(2\pi \cdot \frac{f_{\mathrm{in}}}{f_{\mathrm{s}}}\right). \tag{8}$$

It can be seen that, when f_{in} is close to $n_f \cdot f_{\mathrm{s}}/2$ $(n_f = 0, 1, 2, \ldots)$, $R'(T_{\mathrm{s}})$ becomes approximately 0.

For the kth channel, the correlation difference D_{cor} can be calculated as follows:

$$\begin{aligned} D_{\mathrm{cor-k}} &= N \cdot R'(T_{\mathrm{s}}) \cdot \Delta t_k + E_k \\ &= N \cdot R'(T_{\mathrm{s}}) \cdot \left(\Delta t_k + \frac{E_k}{N \cdot R'(T_{\mathrm{s}})}\right) \end{aligned} \tag{9}$$

where Δt_k is the timing mismatch, and E_k is the error mainly caused by e_{q} and e_{th} [see (3)]. In autocorrelation function $R_{k-1,k}$, an error $E_{k-1,k}$ caused by e_{q} and e_{th} can be expressed as

$$\begin{aligned} E_{k-1,k} = E\left(\begin{array}{l}(y(t_{m,k}) + e_{q,t_{m,k}} + e_{th,t_{m,k}}) \cdot \\ (y(t_{m,k}+\tau) + e_{q,t_{m,k}+\tau} + e_{th,t_{m,k}+\tau})\end{array}\right) \\ - E(y(t_{m,k}) \cdot y(t_{m,k}+\tau)). \end{aligned} \tag{10}$$

In correlation difference $D_{\mathrm{cor-k}}$ of the kth channel, the total error E_k caused by e_{q} and e_{th} can be expressed as

$$\begin{aligned} E_k = (N-k+1) \cdot (E_{1,2} + \cdots + E_{k-1,k}) \\ -(k-1) \cdot (E_{k,k+1} + \cdots + E_{N,1}). \end{aligned} \tag{11}$$

In (9), the term $E_k/(N \cdot R'(T_{\mathrm{s}}))$ in the bracket is the estimation error of the timing mismatch, which is caused by noise. When f_{in} is close to $n_f \cdot f_{\mathrm{s}}/2$, because $R'(T_{\mathrm{s}})$ decreases to 0 as mentioned before, the estimation error in the bracket increases significantly [since $R'(T_{\mathrm{s}})$ is in the denominator of the term in the bracket]. This degrades the calibration accuracy, because the correlation difference $D_{\mathrm{cor-k}}$ is increased.

Usually, the correlation difference D_{cor} is proportional to the timing mismatch Δt, as mentioned before. But this proportional relationship becomes nonlinear when the input frequency is close to the Nyquist frequency $f_{\mathrm{s}}/2$, as Fig. 2 shows. As a result, when the timing mismatch is large (large Δt), the curve will cross with the horizontal axis again (at $\Delta t = -1.7\% \cdot T_{\mathrm{s}}$ in Fig. 2 for example).

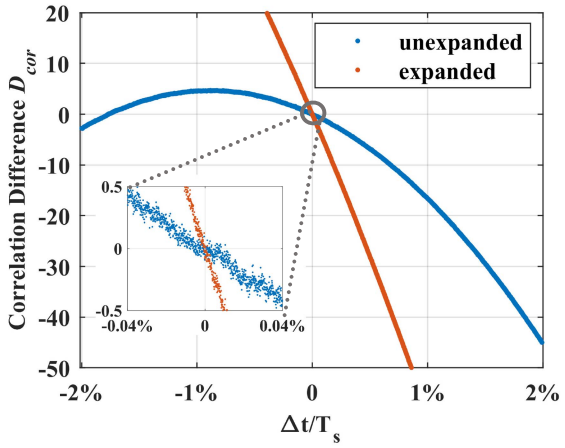

Fig. 3. Correlation difference D_{cor} varies with timing mismatch Δt with expanded and unexpanded interval τ. For expanded interval, $C_{\text{CI}} = 5$.

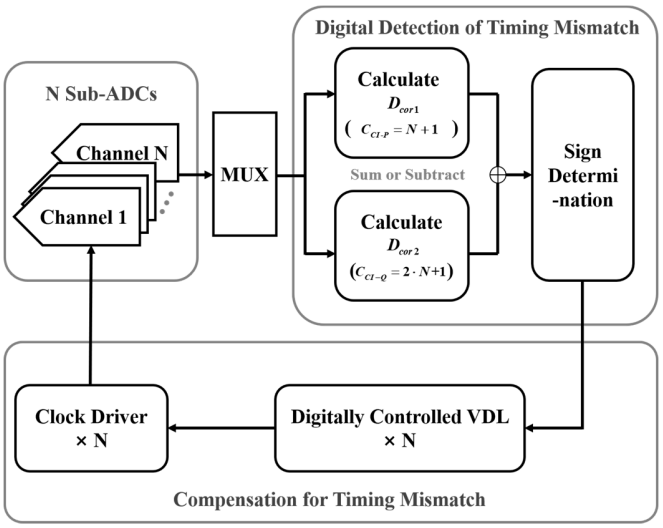

Fig. 4. Block diagram of our calibration mechanism.

This may cause the calibration to converge to a wrong point. Besides, at $\Delta t = 0$, the impact of noise becomes significant, because the D_{cor} is close to zero at this point and the noise is relatively large compared to the value of D_{cor}. This error will degrade the performance of calibration. And the derivative filters cannot distinguish such errors caused by noise. Also, the derivative-based method cannot perform compensation over the entire Nyquist zone due to the limited bandwidth of the filter [12].

C. Proposed Timing Mismatch Calibration Algorithm

To address the above issues, this brief presents a novel timing mismatch background calibration algorithm. It is not sensitive to the frequency because the value of $R'(\tau)$ is increased in the algorithm. The proposed algorithm uses the channels with an expanded interval τ in the autocorrelation function to increase the value of $R'(\tau)$, as discussed below.

Different from using adjacent channels for calibration and $\tau = T_{\text{s}}$ as in [13], $\tau = C_{\text{CI}} \cdot T_{\text{s}}$ is used in this work. Here, C_{CI} is the number of sampling periods in the interval τ for calculating the autocorrelation functions [see (4)]. By expanding the interval τ, the previous $R(T_{\text{s}})$ becomes $R(C_{\text{CI}} \cdot T_{\text{s}})$. By (8), when f_{in} is close to $(n_f \cdot f_{\text{s}}/2)$

$$\begin{aligned} R'\left(C_{\text{CI}} \cdot T_{\text{s}}\right) &= -A^2 \cdot f_{\text{in}} \cdot \pi \cdot \sin\left(C_{\text{CI}} \cdot 2\pi \cdot \frac{f_{\text{in}}}{f_{\text{s}}}\right) \\ &\approx -A^2 \cdot f_{\text{in}} \cdot \pi \cdot C_{\text{CI}} \cdot \sin\left(2\pi \cdot \frac{f_{\text{in}}}{f_{\text{s}}}\right) = C_{\text{CI}} \cdot R'\left(T_{\text{s}}\right). \end{aligned} \tag{12}$$

The value of $|R'(C_{\text{CI}} \cdot T_{\text{s}})|$ becomes approximately C_{CI} times of $|R'(T_{\text{s}})|$. As a result, for the kth channel, the (9) can be rewritten as follows:

$$D_{\text{cor}-C_{\text{CI}}-\text{k}} = C_{\text{CI}} \cdot N \cdot R'\left(T_{\text{s}}\right) \cdot \left(\Delta t_k + \frac{E_k}{C_{\text{CI}} \cdot N \cdot R'\left(T_{\text{s}}\right)}\right). \tag{13}$$

Note that the increased interval τ has no influence on the noise. Thus, the error E_k caused by noise is almost unchanged. As a result, by increasing $R'(\tau)$, the estimation error caused by noise can be reduced effectively [see the term in the bracket in (13)]. Fig. 3 shows that, with the expanded interval, the proposed calibration algorithm has at least five times higher accuracy due to the larger slope of D_{cor} versus Δt as well as the relatively smaller noise. Besides, the nonlinearity in the curve is significantly reduced compared to Fig. 2. As a result, the issue of wrong convergence of Fig. 2 no longer exists in the proposed algorithm.

However, the algorithm with an expanded τ still cannot work at some specific input frequencies. This is because, when $f_{\text{in}} = n_f \cdot f_{\text{s}}/(2 \cdot C_{\text{CI}})$, $n_f = 0, 1, 2, \ldots,$ the value of $R'(C_{\text{CI}} \cdot T_{\text{s}})$ decreases to 0, which is similar to the prior work [see (9)]. This significantly degrades the performance of the proposed algorithm. Similarly, [8]–[11] also have this problem, which suffers from degraded performance at $f_{\text{in}} = n_f \cdot f_{\text{s}}/(2^{n_c})$, $n_c = 1, 2, 4, \ldots, (N/2)$.

To solve this problem in this work, we combine two D_{cor} with two coprime values of C_{CI} ($C_{\text{CI}-\text{P}}$ and $C_{\text{CI-Q}}$). This effectively avoids the small value of derivative $R'(C_{\text{CI}} \cdot T_{\text{s}})$ over the entire Nyquist zone, as will be explained below. First, we calculate the values of $D_{\text{cor}-\text{P}}$ and $D_{\text{cor}-\text{Q}}$, respectively. In our model, we set $C_{\text{CI}-\text{P}} = (N + 1)$ and $C_{\text{CI}-\text{Q}} = (2 \cdot N + 1)$ to make $C_{\text{CI}-\text{P}}$ and $C_{\text{CI}-\text{Q}}$ to be coprime. The next step is to add these two values to get $|D_{\text{cor}-\text{k}}|$, and the sign of $D_{\text{cor}-\text{k}}$ can be set to the same as either $D_{\text{cor}-\text{P}}$ or $D_{\text{cor}-\text{Q}}$, as follows:

$$\begin{cases} |D_{\text{cor}-\text{k}}| = |D_{\text{cor}-\text{P}}| + |D_{\text{cor}-\text{Q}}| \\ \text{sign}(D_{\text{cor}-\text{k}}) = \text{sign}(\text{either} D_{\text{cor}-\text{P}} \text{ or } D_{\text{cor}-\text{Q}}). \end{cases} \tag{14}$$

In this case, the absolute value of $R'(\tau)$ in $D_{\text{cor}-\text{k}}$ can be expressed as

$$|R'(\tau)| = |R'(P \cdot T_{\text{s}})| + |R'(Q \cdot T_{\text{s}})|. \tag{15}$$

Because $|R'(\tau)|$ is the sum of two enlarged values, the issues of noise and high-order nonlinearity will be suppressed [similar to the term in the bracket of (13)]. Besides, since $C_{\text{CI}-\text{P}}$ and $C_{\text{CI}-\text{Q}}$ are coprime, the values of $|R'(P \cdot T_{\text{s}})|$ and $|R'(Q \cdot T_{\text{s}})|$ will never be zero simultaneously. This ensures that $|R'(\tau)|$ is always not zero over the Nyquist Zone. As a result, the issue of degraded estimation accuracy at some specific input frequencies no longer exists in this work.

Finally, we need to consider how to adjust the correlation difference D_{cor} to zero, because D_{cor} is proportional to the timing mismatch as mentioned before, and zero D_{cor} means zero timing mismatch. In this work, we use the VDLs for adjusting the D_{cor}, due to its low power consumption. Also, unlike the derivative filter which cannot work at high frequency due to its limited bandwidth, the VDL can perform compensation at any input frequency. Fig. 4 shows the proposed

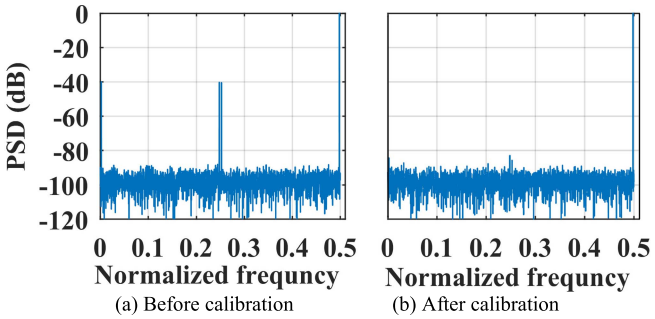

Fig. 5. Simulated output spectrum for a four-channel 12-bit TI ADC. (a) Before and (b) after applying calibration for $f_s = 1$ GHz and $f_{in} = 2039/4096 \cdot f_s$.

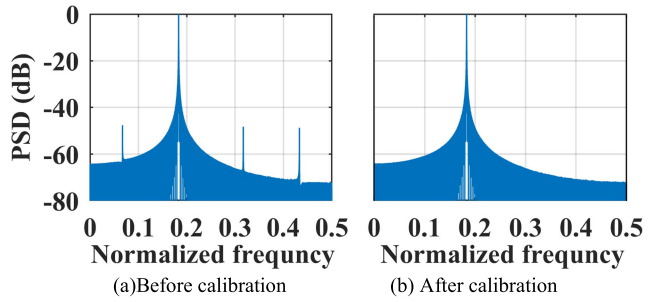

Fig. 6. Simulated output spectrum (a) before and (b) after calibration for the 1GSps four-channel 12-bit TI ADC with a BPSK input. Here, we use the PRBS data modulated with BPSK modulation as the input to show the communication signals. In the BPSK input, the carrier frequency is 0.0.183 and the code rate is 0.00015 in normalized frequency.

calibration process using the digitally controlled VDL. The advantage of our algorithm is the calibration with improved accuracy at any input frequency. Another advantage is the low complexity. For a 12-bit ADC, when $C_{CI-P} = (N+1)$ and $C_{CI-Q} = (2 \cdot N + 1)$, N multiply-accumulators and $12 \cdot N \cdot (N+2)$ flip-flops working at (f_s/N) are needed. The complexity is much smaller than the method of calculating high-order Taylor series approximation, such as [12].

III. Simulation Results

To verify the proposed calibration algorithm, a behavior model of four-channel 12-bit TI ADC is designed. It has non-ideal effects, including the timing mismatch, the clock jitter, and the thermal noise. The timing mismatch is 0, $-0.19\% \cdot T_S$, $-0.60\% \cdot T_S$, and $0.88\% \cdot T_S$ for the four channels, respectively; the rms jitter is $200\,f_s$; and the thermal noise leads to an SNR of 74.5 dB for the input signal. To trim the timing mismatch in the model, a VDL with a time resolution of $21\,f_s$ is used. Each step size of the VDL is determined through the post-layout simulation, so that the ADC model is more realistic. The calibration converges after ten calibration cycles and each cycle takes 20.48 k samples to calculate correlation functions for high-precision estimation.

With an input at $f_{in} = (2039/4096) \cdot f_s$, the output spectrum before and after calibration is shown in Fig. 5. It can be seen that the proposed calibration effectively reduces the spurs caused by timing mismatch, even if the input frequency is close to the Nyquist frequency. The SNDR is increased from 35.5 to 63.3 dB, and the SFDR is increased from 40.0 to 84.6 dB.

Fig. 6 shows the spectrum of a binary phase shift keying (BPSK) input before and after calibration, which demonstrates that the proposed algorithm could work with angle-modulated communication

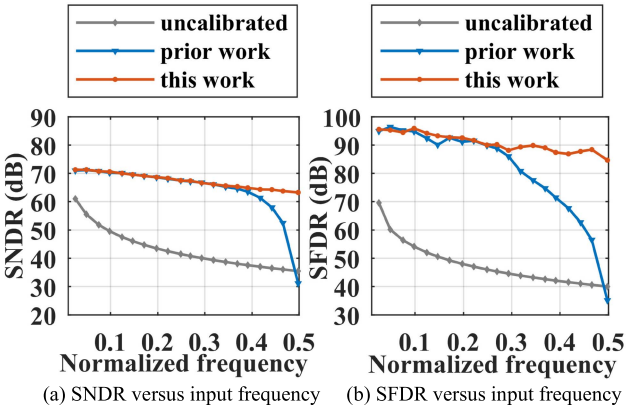

Fig. 7. (a) SNDR and (b) SFDR of the 1GSps 12-bit four-channel TI ADC before and after applying calibration at different frequencies.

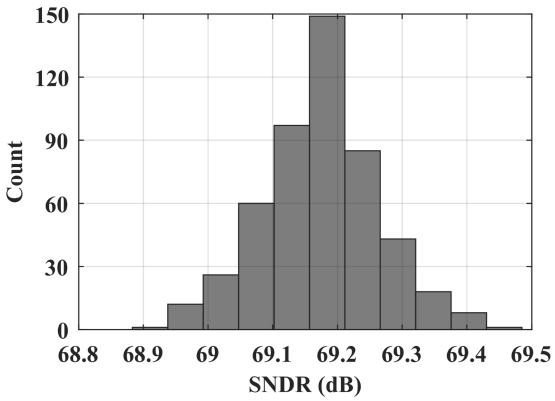

Fig. 8. Monte Carlo simulation results for the 1GSps 12-bit four-channel at $f_{in} = 701/4096 \cdot f_s$.

signals. As can be seen, the proposed algorithm can effectively suppress the spurs brought by timing mismatches.

Fig. 7 shows the SNDR and SFDR versus input frequency by using the proposed calibration algorithm and the prior algorithm of [13]–[14] based on derivative. As can be seen, when the input frequency is close to the Nyquist frequency, the proposed algorithm still has a good performance. By contrast, the SNDR and SFDR of prior algorithm are decreased significantly, even if we use ideal derivative filters in the model. Also, the prior work cannot perform the calibration at high frequency in practice due to the limited bandwidth of filters, whereas the compensation in this work through VDL can work at any frequency. Overall, compared to the prior work, the proposed algorithm improves the SNDR and SFDR by up to 32.2 and 49.5 dB, respectively.

Fig. 8 shows a Monte Carlo simulation result after calibration. The timing mismatch is set to $3\sigma = 3\% \cdot T_s$ in each channel. It can be seen that the SNDR after calibration is at least 68.88 dB and the mean value of SNDR is 69.17 dB.

Table I compares the proposed algorithm with the state-of-the-art algorithms of recent years. Wei *et al.* [9] have a limitation on its input frequency. The calibration performance is degraded at $f_{in} = n_f \cdot f_s/(2^{n_c})$ $(n_c = 1, 2, 4, \ldots, N/2)$. And the number of channels in [9] is strictly limited to the power of 2, with the cumbersome calibration process. Besides, Yin and Ye [7] and Salib *et al.* [12] have degraded SNDR and SFDR when f_{in} is close to the Nyquist frequency. Furthermore, the estimation method in [5] is not blind. It requires an extra reference ADC, whose performance determines

TABLE I
SUMMARY AND COMPARISON OF THE ALGORITHMS

	[5] TCASII 2020	[7] TCASII 2020	[9] JSSC 2014	[12] TCASI 2019	**This work**
Resolution	12	12	8	12	**12**
Channels	4	4	4	4	**4**
Arbitrary Channel Calibration	Yes	Yes	No	Yes	**Yes**
All channels calibrated at the same time	Yes	Yes	No	Yes	**Yes**
Blind Estimation	No	Yes	Yes	Yes	**Yes**
Limitation on the Frequency of Input Signals	No	Yes	Yes	Yes	**No**
Convergence Time (samples)	N/A	3.1k	240k	1310k	**204.8k**
Rms Jitter Applied (fs)	N/A	N/A	N/A	N/A	**200**
SNR of input signal (dB)	N/A	N/A	N/A	68	**72**
SNDR (dB)	66.0 @ $0.375\,f_s$ 65.0 @ $0.475\,f_s$ (Behavior model)	<60.0 @ $0.300\,f_s$ <50.0 @ $0.400\,f_s$ (Behavior model)	45.0 @ $0.175\,f_s$ 44.4 @ $0.473\,f_s$ (Measure-ment)	65.2 @ $0.420\,f_s$ <50.0 @ $0.490\,f_s$ (Behavior model)	**64.3 @ $0.420\,f_s$** **63.25 @ $0.498\,f_s$** (Behavior model)
SFDR (dB)	80.0 @ $0.375\,f_s$ 72.0 @ $0.475\,f_s$ (Behavior model)	<60.0 @ $0.300\,f_s$ <50.0 @ $0.400\,f_s$ (Behavior model)	N/A	90.0 @ $0.420\,f_s$ <50.0 @ $0.490\,f_s$ (Behavior model)	**86.9 @ $0.420\,f_s$** **84.6 @ $0.498\,f_s$** (Behavior model)

the calibration accuracy. By contrast, the proposed algorithm solves all of the above issues. It can perform the calibration with improved accuracy at any input frequency, and under an arbitrary number of channels. Also, all the channels can be calibrated simultaneously, without the need for any extra reference channel.

IV. CONCLUSION

In this brief, a novel timing mismatch background calibration algorithm for TI ADCs is presented. It can calibrate an arbitrary number of channels with an arbitrary input frequency. By applying the autocorrelation functions with an expanded interval, the algorithm increases the calibration accuracy. Besides, the proposed algorithm prevents the small derivative values in the correlation difference from degrading the skew estimation accuracy. Compared to prior works, this algorithm has at least five times better detection accuracy when the frequency of the input signal is close to the Nyquist frequency. In addition, this work has no requirement for any extra reference ADC and calculating the high-order statistics.

REFERENCES

[1] W. C. Black and D. A. Hodges, "Time interleaved converter arrays," *IEEE J. Solid-State Circuits*, vol. JSSC-15, no. 6, pp. 1022–1029, Dec. 1980.

[2] D. G. Nairn, "Time-interleaved analog-to-digital converters," in *Proc. IEEE Custom Integr. Circuits Conf.*, San Jose, CA, USA, Sep. 2008, pp. 289–296.

[3] Q. Lei, Y. Zheng, D. Zhu, and L. Siek, "A statistic based time skew calibration method for time-interleaved ADCs," in *Proc. IEEE Int. Symp. Circuits Syst. (ISCAS)*, Jun. 2014, pp. 2373–2376.

[4] Y. Zhou, B. Xu, and Y. Chiu, "A 12-b 1-GS/s 31.5-mW time-interleaved SAR ADC with analog HPF-assisted skew calibration and randomly sampling reference ADC," *IEEE J. Solid-State Circuits*, vol. 54, no. 8, pp. 2207–2218, Aug. 2019.

[5] S. Azizian and M. Ehsanian, "Generalized method for extraction of offset, gain, and timing skew errors in time-interleaved ADCs," *IEEE Trans. Circuits Syst. II, Exp. Briefs*, vol. 67, no. 7, pp. 1214–1218, Jul. 2020.

[6] C.-C. Huang, C.-Y. Wang, and J.-T. Wu, "A CMOS 6-bit 16-GS/s time-interleaved ADC using digital background calibration techniques," *IEEE J. Solid-State Circuits*, vol. 46, no. 4, pp. 848–858, Apr. 2011.

[7] M. Yin and Z. Ye, "First order statistic based fast blind calibration of time skews for time-interleaved ADCs," *IEEE Trans. Circuits Syst. II, Exp. Briefs*, vol. 67, no. 1, pp. 162–166, Jan. 2020.

[8] B. Razavi, "Design considerations for interleaved ADCs," *IEEE J. Solid-State Circuits*, vol. 48, no. 8, pp. 1806–1817, Aug. 2013.

[9] H. Wei, P. Zhang, B. D. Sahoo, and B. Razavi, "An 8 bit 4 GS/s 120 mW CMOS ADC," *IEEE J. Solid-State Circuits*, vol. 49, no. 8, pp. 1751–1761, Aug. 2014.

[10] M. Straayer *et al.*, "27.5 A 4 GS/s time-interleaved RF ADC in 65 nm CMOS with 4 GHz input bandwidth," in *IEEE Int. Solid-State Circuits Conf. (ISSCC) Dig. Tech. Papers*, Jan. 2016, pp. 464–465.

[11] S. Devarajan *et al.*, "16.7 A 12b 10 GS/s interleaved pipeline ADC in 28 nm CMOS technology," in *IEEE Int. Solid-State Circuits Conf. (ISSCC) Dig. Tech. Papers*, Feb. 2017, pp. 288–289.

[12] A. Salib, M. F. Flanagan, and B. Cardiff, "A high-precision time skew estimation and correction technique for time-interleaved ADCs," *IEEE Trans. Circuits Syst. I, Reg. Papers*, pp. 1–14, 2019.

[13] H. Le Duc, D. M. Nguyen, C. Jabbour, P. Desgreys, O. Jamin, and V. Tam Nguyen, "Fully digital feedforward background calibration of clock skews for sub-sampling TIADCs using the polyphase decomposition," *IEEE Trans. Circuits Syst. I, Reg. Papers*, vol. 64, no. 6, pp. 1515–1528, Jun. 2017.

[14] J. Matsuno, T. Yamaji, M. Furuta, and T. Itakura, "All-digital background calibration technique for time-interleaved ADC using pseudo aliasing signal," *IEEE Trans. Circuits Syst. I, Reg. Papers*, vol. 60, no. 5, pp. 1113–1121, May 2013.